

Magneto-optical studies of the type-I/type-II crossover and band offset in ZnTe/Zn_{1-x}Mn_xTe superlattices in magnetic fields up to 45 T

H. H. Cheng, R. J. Nicholas, and M. J. Lawless

Department of Physics, Clarendon Laboratory, University of Oxford, Parks Road, Oxford OX1 3PU, United Kingdom

D. E. Ashenford and B. Lunn

Department of Engineering Design and Manufacture, Hull University, HU6 7RX Humberside, United Kingdom

(Received 21 April 1995)

We report measurements of magnetorefectivity in ZnTe/Zn_{1-x}Mn_xTe superlattices with varying well width in magnetic fields up to 45 T. From an analysis of the Zeeman splitting, we investigate the change of band alignment with field and the band offset ratio. A crossing of the 1s exciton transitions from the ZnTe buffer layer and the 1s heavy hole σ_+ exciton of the superlattice is observed, providing unambiguous evidence of a band alignment change from type I to type II. The excitonic energy levels for both type-I and type-II band structure are calculated using a variational method. This model fits the experimental data very well at high fields for both σ_+ and σ_- transitions and predicts that the type-I/type-II crossover occurs at 2–3 T. Also by fitting the σ_+ transition energy as a function of field a conduction band offset ratio of $\Delta E_c/\Delta E_g=0.72\pm 0.04$ is deduced.

I. INTRODUCTION

The zinc-blende material Zn_{1-x}Mn_xTe is one of the Mn-based dilute semimagnetic semiconductor (DMS) family, but has been less studied than the other members. So far, magneto-optical experiments on this material have been reported only on bulk single crystals.^{1,2} Following recent progress made with the molecular beam epitaxy (MBE) growth technique for this material, it is now possible to study the electronic structure of ZnTe/Zn_{1-x}Mn_xTe superlattices (SL's). This system has a large magnetic tuning of the band edge in the semimagnetic layers, due to the *sp-d* exchange interaction. Compared with other DMS materials, such as CdTe/Cd_{1-x}Mn_xTe, the present system has two major advantages for studying band alignment modulation: (a) the change of band gap with Mn concentration is small, only one half of that of Cd_{1-x}Mn_xTe. The valence band offset is therefore small. (b) The exchange coupling constant is large, resulting in a large band edge modulation of the band alignment with magnetic field. It is 20% larger than that of Cd_{1-x}Mn_xTe. We have, therefore, used this system to study the magneto-optical characteristics of the field-induced band alignment change from type I to type II.

The characteristics of the type-I/type-II crossover have been a debatable topic for the past few years, due to the complications introduced by the Coulomb interaction (the binding energy of the 1s, heavy hole is typically of order of 20 meV). Experimental evidence has been reported on two types of system: (a) CdTe/Cd_{0.93}Mn_{0.07}Te quantum wells in which the valence band offset is comparable to exciton binding energy,^{3,4} (b) the "spin superlattice" of ZnSe/Zn_{1-x}Fe_xSe and ZnSe/Zn_{1-x}Mn_xSe in which the conduction band offset is small and valence band offset is nearly zero.^{5,6} In both cases, the data are

limited to the low-field regime (≤ 8 T), where the strong Coulomb energy significantly modulates the confinement potential, in particular, for the valence band.

In this paper, we present an interband magnetorefectivity study of four ZnTe/Zn_{1-x}Mn_xTe superlattices (SL's) with different well widths in fields up to 45 T. This enabled us to examine both the low-field regime and, in particular, the high-field regime in which the magnetic interaction dominates. We have observed a crossing of the 1s excitonic transition from the ZnTe buffer layer with the 1s heavy hole σ_+ component of the superlattice, providing clear experimental evidence of the band alignment change from type I to a type II. A theoretical calculation of the excitonic Rydberg energy and diamagnetic shift for both type-I and type-II band structure is performed to quantitatively interpret the data. The model fits the σ_- transition very well up to 45 T, and gives a good fit to the σ_+ component at very low fields and above ≈ 15 T. This suggests that a "strong" field-induced type-II band alignment for the $m_j = -3/2$ spin state will only occur in the high-field regime, where the field-dependent valence band edge modulation dominates the Coulombic energy, and that an intermediate regime exists where there is a competition between the Coulomb interaction and superlattice potential. Based on the analysis of the energy shift of the σ_+ transition at high field, the band offset ratio of this system is deduced.

II. EXPERIMENTAL RESULTS

A series of SL samples were grown by MBE on lattice matched GaSb substrates. They consist typically of a thick (2000 Å) ZnTe buffer layer and then ten alternating layers of ZnTe and Zn_{1-x}Mn_xTe. Long period structures were studied, with thick barriers (150 Å) with the Mn

content of 7% and well widths of nominally 40, 60, 80, and 100 Å. The precise layer thicknesses were measured by x-ray scattering. Magnetorefectivity was studied in the Faraday configuration (B perpendicular to the SL plane) using long pulse (10 msec) magnetic fields up to 45 T, and a pulsed light source (Hg vapor lamp) fired at the peak field for a period of 500 μ sec. The samples were placed in the pulsed field center and immersed in liquid helium. The reflected light was collected using a fiber bundle and analyzed using a 0.25 m spectrometer and nitrogen cooled CCD detector. Measurements were also performed using polarized light in a steady field up to 15 T. This gives a clear identification of the σ_+ and σ_- transitions at low field with a fine resolution for the field interval, which is important for studying the change of transition energy around the type-I/type-II crossover region.

The zero-field spectra for the four samples are shown in Fig. 1. These spectra are ratioed against a mirror response of the light source, and show a sharp minimum (or maximum) for the excitonic features around the region of both the barrier and SL band gap. The SL transition can give rise to both maxima and minima in the reflectivity, depending on the overall phase of the interference structure from the layers. The assignment of maxima or minima to the precise transition features was made using the full family of the magnetorefectivity spectrum (cf. Fig. 2.), where the presence of peak sharpening generally made the specific assignment unambiguous. The feature at 2383.3 meV is due to the $1s$ exciton of the buffer layer. Two transition features around the band gap of $\text{Zn}_{1-x}\text{Mn}_x\text{Te}$ can be identified due probably to differences in the manganese concentration in the semi-magnetic barriers. The observed SL transitions are the heavy hole (HH) to the ground state of the conduction band ($E1$) and light hole (LH) to $E1$ exciton, labeled as 1HH, 1LH, respectively. As the well width decreases, the energy of the 1HH and 1LH transitions move upwards due to the confinement effect. The potential height that determines the confinement energy depends on the band offset ratio and the strain due to the lattice mismatch of ZnTe and $\text{Zn}_{1-x}\text{Mn}_x\text{Te}$. The strain, for the sample structure studied here, is accommodated in the magnetic

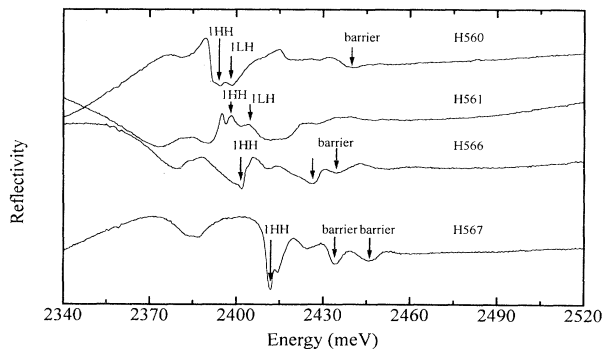


FIG. 1. Zero-field reflectivity spectra of the four samples showing the transition energy assignments for 1HH and 1LH.

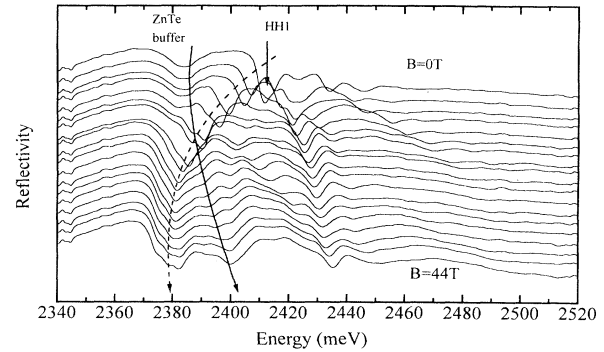


FIG. 2. A family of reflectivity spectra in pulsed field from 0 to 44 T for H567. The dashed line (solid line) indicates the $1s$ HH transitions in the superlattice (and bulk ZnTe) buffer layer.

layers as biaxial compression, whereas the quantum wells (nonmagnetic layers) are not strained, due to the lattice match with the buffer layer. This lifts the degeneracy at the zone center for the barriers resulting in different potential heights for HH and LH in the quantum well. A summary of the transition energies and fitted parameters is given in Table I.

In the table, the Mn^{2+} concentrations in the barrier layers are determined from the bulk $\text{Zn}_{1-x}\text{Mn}_x\text{Te}$ transition energies ($B=0$) using the expression, $E(\text{barrier}) = E_g + 806 \cdot x - E_{\text{bulk}}$ in meV, where 806 is the constant characterizing the change of band gap with manganese concentration, E_{bulk} is the calculated bulk (ZnTe) exciton binding energy of 14.1 meV. The positive conduction band (CB) and valence band (VB) offsets show that the system has a type-I structure at zero field. The measured well/barrier width is obtained from the x-ray measurement and, the fitted values are deduced from the fitting of the HH exciton, using the exciton model discussed later.

Reflectivity spectra in pulsed magnetic fields for sample H567 are shown in Fig. 2. The zero-field transitions from the barrier and SL split into two components with applied magnetic fields corresponding to the σ_+ ($m_{hj} = -3/2$ to $m_{ej} = -1/2$) and σ_- ($m_{hj} = +3/2$ to $m_{ej} = +1/2$) transitions. In Fig. 2, we mark the movement with the field of two of the transitions. The solid line indicates the ZnTe buffer transition and the dashed line indicates the HH lower branch. Other features can be seen but their movement with field is not indicated. We first discuss the field-dependent spectra of the transitions from the thick magnetic layers. On applying external field, the transition feature at zero field splits symmetrically (Zeeman splitting) due to the spin-dependent $sp-d$ exchange interaction. With increasing applied field, the σ_- component moves to higher energy and becomes broader and weaker, due to the presence of small fluctuations of the manganese concentration, while for the σ_+ component, the opposite occurs. The energy shift, in the Faraday configuration, is described by Gaj:⁷

TABLE I. Summary of zero-field transition energies and fitted well and barrier widths.

Sample name	Mn (%)	CB (VB) offset HH (meV)	HH1- E_1 (meV)	LH1- E_1 (meV)	Measured well/barrier (\AA)	Fitted width (\AA)	E_b (HH) (meV)
H560	7	54.6 (11.1)	2393.8	2398.0	100/150	100/150	19.5
H561	6.5	50.3 (10.2)	2397.6	2403.7	80/150	80/150	20.0
H566	7	54.0 (11.0)	2401.0		65/150	71/150	20.5
H567	7.5	59.2 (10.6)	2411.1		48/150	51/150	20.8

$$\begin{aligned}\Delta E_c &= m_{ej} N_0 \alpha \langle S_z(B) \rangle, \\ \Delta E_v &= m_{hj} N_0 \beta \langle S_z(B) \rangle,\end{aligned}\quad (1)$$

where m_{ej} , m_{hj} are the carrier spin components in the SL direction of the CB and VB, $N_0\alpha$ $N_0\beta$ are the coupling constants for electrons and holes and $\langle S_z(B) \rangle$ is the macroscopic mean spin value. At high field, the σ_+ transition shifts downwards slowly, because of the cancellation of the spin splitting and the diamagnetic shift of the $1s$ exciton. The total exchange splitting is ≈ 70 meV at 45 T, estimated from the σ_+ component and using the diamagnetic shift observed from the ZnTe buffer layer of ≈ 18 meV. In contrast to the paramagnetic model proposed by Gaj, where the exchange splitting saturates at moderate field, the Zeeman splitting continues to increase with field indicating the suppression of the antiferromagnetic interaction of Mn^{2+} ions at high field as is well known in other Mn II-VI alloys.^{8,9}

The field-induced exchange splitting of the magnetic layer band edge results in an ‘‘effective potential height’’ for the different spin states in the quantum well, where the zero-field potential height is modified by the energy shift of Eq. (1). As a consequence the SL features show an asymmetric splitting for the σ_+ and σ_- components. The σ_- transition of the HH moves continuously upward with increasing field up to 45 T, due to the increase of the effective confinement potential for both spin states of the CB and VB. For the σ_+ component, it moves downward rapidly at low field, with a rate of ≈ 4 meV/T indicating the rapid decrease of the carrier confinement potentials. With increasing field, at around 6 T, the buffer (bulk ZnTe) $1s$ exciton shifts upwards and crosses the HH transition, providing unequivocal evidence of the ob-

servation of a type-I/type-II band alignment crossover. Similar crossing behavior is also observed for the other three samples. Above the crossover field, the $1s$ buffer exciton progressively moves upward, due to its diamagnetic shift, while the HH transition continues to decrease and fall further below the band gap of ZnTe (about 20 meV below by 45 T). Above 15 T, the HH energy position remains almost constant up to 45 T, due to the cancellation of the valence band gap modulation and the diamagnetic shift. The HH feature also broadens and begins to split at high field, possibly due also to fluctuation of the Mn alloy content in the magnetic layers. It is not possible to analyze accurately the change of oscillator strength with field, due both to the additional small splitting and the crossing with the buffer transition. The energy shift of both components of the HH at 15 T and the transition field (B_t), where buffer $1s$ exciton crosses the HH lower branch for the four samples, is listed in Table II. The Zeeman splitting shows an increase with decreasing well width, due to the increasing barrier penetration for the narrow well at zero field. For the LH exciton, the transition feature becomes very much broader and weaker with increasing field and mixes with the σ_+ component of the barrier transition at around 4 T. In this paper, we concentrate on the HH exciton, since we are interested in the type-I/type-II crossover and the lower component of the HH exciton is the lowest transition.

III. THEORY

To quantitatively interpret the interband optical transition energies of the type-I and type-II excitons, a theoretical calculation of the excitonic energy levels using the effective mass approximation is performed. The detail of

TABLE II. Energy shift of σ_- and σ_+ HH1 components at 15 T and the transition field B_t , where the ZnTe $1s$ exciton and HH1 SL exciton cross. B_c is the calculated value, where band alignment changes from type I to type II. The last column is the transition energy of the σ_+ component at high field (45 T).

Sample name	Energy shift σ_- (σ_+) component (meV)	Transition field B_t (T)	Calculated B_c (T)	Transition energy at high field (meV)
H560	3.8 (11.7)	7	3-4	2382.4 (2376.5)
H561	5.3 (17.0)	6	2-3	2380.8
H566	9.8 (23.8)	6	2-3	
H567	18.0 (29.3)	6	2-3	2381.7 (2377.8)

the model is published elsewhere.¹⁰ Here, we describe the change of the energy levels of the exciton with field and, in particular, the behavior of the type-II exciton. The exciton Hamiltonian is written in cylindrical coordinates in the following form:^{11,12}

$$H = \frac{-\hbar^2}{2\mu_{\parallel}} \left[\frac{1}{\rho} \frac{\partial}{\partial \rho} \rho \frac{\partial}{\partial \rho} + \frac{1}{\rho^2} \frac{\partial^2}{\partial \phi^2} \right] - \frac{\hbar^2}{2m_e^*} \frac{\partial^2}{\partial z_e^2} - \frac{\hbar^2}{2m_h^*} \frac{\partial^2}{\partial z_h^2} + V_e(z_e, m_{ej}) + V_h(z_h, m_{hj}) - \frac{e^2}{4\pi\epsilon[\rho^2 + (z_e - z_h)^2]^{1/2}} + \frac{1}{8}\mu_{\parallel}\omega^2\rho^2, \quad (2)$$

where m_e^* , m_h^* are the effective masses of conduction electrons and heavy holes along the quantum confinement direction (z), μ_{\parallel} is the exciton reduced effective mass in the SL layer plane, $\omega = eB/\mu_{\parallel}$ is the cyclotron frequency, and ϵ is the dielectric constant. $V_e(z_e, m_{ej})$, $V_h(z_h, m_{hj})$, are the square well potential for electrons and holes, respectively, which are strongly field dependent due to the energy shift of the barrier layers described in Eq. (1). To include the effect of strain, the zero-field potential depth is modified by

$$\begin{aligned} \Delta V_c &= a_c(2 - D)\epsilon^{\parallel}, \\ \Delta V_v &= a_v(2 - D)\epsilon^{\parallel} \pm b_v(1 + D)\epsilon^{\parallel}, \end{aligned} \quad (3)$$

where a_c (a_v) is the hydrostatic deformation potential of the conduction (valence) band, b_v is the shear deformation potential, ϵ^{\parallel} is the strain in the layer plane, and D is the elastic coefficient defined from the elastic constants C_{12} and C_{11} ($D_{[001]}=2C_{12}/C_{11}$). The plus and minus signs correspond to the HH and LH. The strain parameters for ZnTe are taken from Ref. 13 and we use the same values for $\text{Zn}_{1-x}\text{Mn}_x\text{Te}$, due to the low Mn concentration. In the calculation of the SL excitonic energy levels, the energy shift of the quantum well band edge is taken from the value observed for the barrier layers as an input to the program. The in-plane electron effective mass is increased slightly with the applied field to account for nonparabolicity effects using $m^*/m(E) = 1 + [K_2 eB/2E_g m^*]$, where K_2 is the nonparabolicity factor taken from Ref. 14.

The exciton Hamilton of Eq. (2) is solved by the variational method, using a wave function of $\phi = f_e(z_e) f_h(z_h) g(\lambda, \rho, z_e - z_h)$, where f_e (f_h) is the electron (hole) ground state of the potential well with an energy eigenstate of E_e (E_h) and g is the trial function chosen as a simple harmonic function $\exp(-\lambda^2[\rho^2 + (z_e - z_h)^2])$.¹⁵ The Rydberg energy (E_b) of the 1s state is obtained by subtracting the minimum expectation value of the Hamiltonian [without the in-plane magnetic field term of Eq. (2)] from the subband energy of the electrons and holes determined from the subband calculation. The diamagnetic shift (E_{dia}) is then defined as the change of effective Rydberg, due to the applied in-plane field.

IV. ANALYSIS AND DISCUSSION

Based on the above description, the field-dependent interband transition energies ($E = E_g + E_e + E_h - E_b$

+ E_{dia}) are calculated for the two HH transitions. The characteristic shift of the σ_- component can be categorized into two regions in which (a) at low field the diamagnetic shift is small and the band edge modulation of the SL dominates the change of the excitonic energy levels and (b) at high field, where the diamagnetic shift dominates. For the σ_+ component, at low fields, the large magnetic interaction rapidly raises the valence band edge of the magnetic layers and thus leads to the formation of a type-II band structure, resulting in a rapid decrease of the binding energy, due to the spatial separation of electrons and holes. The field strengths (B_c) necessary to cause the crossover in the band alignment, using a conduction band offset ratio $\Delta E_v/\Delta E_g$ (Q_c) of 0.72 and Eq. (1) are listed in Table II. For all the samples studied here, it occurs at roughly the same value of ≈ 3 T, because of the similar values of manganese concentration. At high field, the change of confinement energy of the electrons and holes with field is relatively small compared with the diamagnetic shift due to the slow change in band edge modulation and wider well thickness for the hole (the hole is localized in the magnetic layers of thickness 150 Å). As a consequence, the energy shift is dominated by the type-II band gap modulation and the diamagnetic shift.

In Fig. 3, the measured transition energies of sample H560 are plotted with the calculated values using effective masses of $m_e^*=0.134$, $m_{h\perp}^*=0.5$, $m_{h\parallel}^*=0.45$, and $Q_c=0.72$, where $m_{h\perp}^*$ is the hole effective mass in the SL direction and $m_{h\parallel}^*$ is the in-plane (x - y) mass. The accuracy of these parameters will be discussed below, here, we first discuss the results of the fitting. The fit shows a very good agreement for the σ_- component, which has a

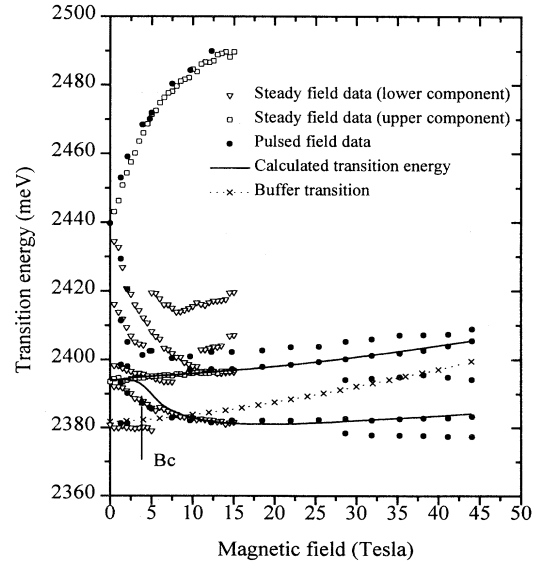


FIG. 3. Experimental transition energies as a function of magnetic field for sample H560 (100/150 Å) and fitted energies (solid line), using the calculations described in the text with $Q_c=0.72$.

diamagnetic shift of about half of that the bulk $1s$ exciton (≈ 9 meV). This is expected for the type-I exciton, because of the increase in confinement energy with field and the reduced dimensionality of the exciton. For the σ_+ component, the calculated transitions agree at very low field and show a small bump around the crossover region, while the data do not show this characteristic clearly, falling a couple of meV below the calculations. The disagreement comes from the fact that the valence band offset is very small around this region and the variational form of the exciton is probably a rather poor approximation. However, as the electronic structure becomes more clearly defined as a type-II band alignment with increasing field, the differences between the data and the calculated values reduces and the two agree well above 15 T, suggesting that the SL band edge modulation has overcome the Coulomb interaction. In Fig. 4, the valence band offset (VBO) is plotted as a function of applied magnetic field for the $-3/2$ HH state, which shows that above 15 T the HH potential depth is more than three times the type-II exciton binding energy (≈ 9 meV) and, therefore, the strong confinement localizes the hole in the magnetic layers. In the figure, a positive (negative) VBO represents a type-I (type-II) band structure. The calculated diamagnetic shift is also plotted in Fig. 4 showing that, above 15 T the change of the well depth, and hence the effective band gap, due to the exchange interaction is nearly the same as E_{dia} . This results in very little net change of the transition energy which is consistent with the experimental data. All the samples studied at high field have a similar transition energy (≈ 2380 meV) for the HH σ_+ component (Table II). This is because of their similar Mn^{2+} concentration and the wide thickness of the $\text{Zn}_{1-x}\text{Mn}_x\text{Te}$ layer. The small differences in width between different samples (from 150

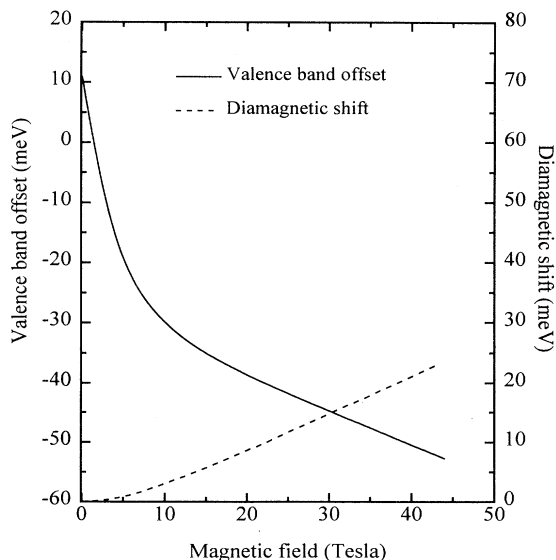


FIG. 4. The valence band offset for a sample with $x=7\%$ and the diamagnetic shift of sample H560.

\AA of sample H560 to 140 \AA of H567) only shift E_{dia} by a couple meV.

A pronounced type-II band alignment would be expected to lead to a significant reduction in the exciton oscillator strength. Even at high field however, the hole wave function is by no means wholly confined in the magnetic layers, but still penetrates significantly into the non-magnetic layers. The degree of penetration in the SL direction depends on the barrier height of the quantum well, which increases with applied field, resulting in an overlap of the electron and hole wave function of $\approx 17\%$ of the zero-field value at 45 T. The oscillator strength also depends on the in-plane carrier motion. In contrast to the SL direction, the overlap in the $(x-y)$ plane increases with applied field, due to the reduction of the carrier cyclotron radius with field, and by 45 T, we expect a more than doubling of the overlap. As a result, the combination of these two opposite effects gives only a relatively small change in oscillator strength. This is qualitatively consistent with the data, however, it is not feasible to make an accurate comparison with experiment due to the mixing of the SL signal with that of the $1s$ buffer exciton, as mentioned above.

In modeling the excitonic splitting of the HH as described above, both the value of the hole effective mass and, in particular, the band offset ratio are used as modeling parameters. The effective HH mass is deduced from fitting of the σ_- exciton transition. As we have discussed, the change of the excitonic transition energy is dominated by the change of confinement energy at low field and by E_{dia} at high field. This gives largely independent measurements of both the longitudinal and in-plane effective masses of the hole. Since the strength of the band

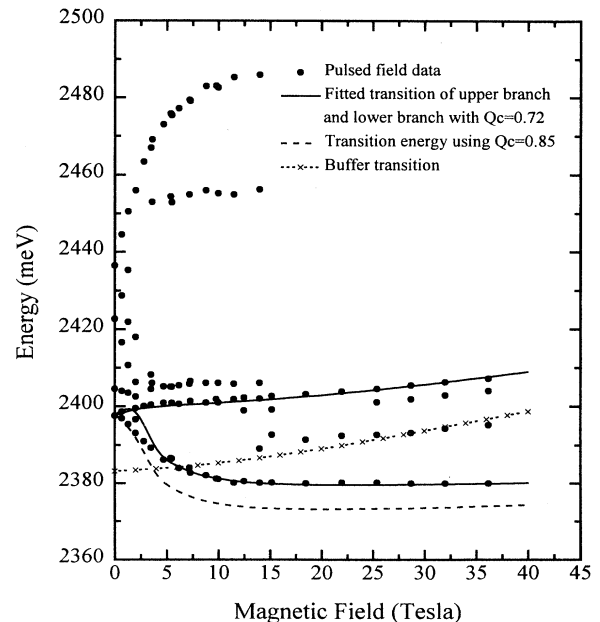


FIG. 5. Experimental transition energies as a function of magnetic field for sample H561 (80/150 \AA) and fitted energies using $Q_c=0.72$ (solid line) and 0.85 (dashed line).

edge tuning of the valence band is about five times larger than the conduction band, the change of confinement energy at low field comes mainly from the valence band, and hence measures the longitudinal hole effective mass, whereas the diamagnetic shift at high field is more sensitive to the in-plane mass. (The electron mass is taken from Ref. 14.) For the LH effective mass, a fitting to the field-dependent transition energies is difficult, due to both the broad features of the spectrum and the mixing with the σ_+ component of the bulk transition. The resulting HH effective mass in the SL direction of (0.50) is very close to the values of 0.48 reported by Said and Kanehisa,¹⁶ but the in-plane mass value is significantly higher (0.44) than their value of 0.22. Such high in-plane hole masses are frequently observed from the fitting of interband transitions at high fields.¹⁷

Using this set of band mass parameters, the conduction band offset ratio is determined by fitting the σ_+ transition. In Fig. 5, the results of a calculation with different band offset ratios is compared with experimental data for sample H561, illustrating that at high fields, a good fit is obtained by using $Q_c=0.72$. The fitting shows that, around the crossover region where the calculation is less reliable, the shoulder appearing with $Q_c=0.72$ (solid line) is smeared out by using the larger conduction band offset ratio of 0.85 (dashed line). Similar behavior has led several authors to interpret such a smooth transition from low-field data by using a large Q_c value in the CdTe/Cd_{1-x}Mn_xTe system.^{18,19} However, as shown in Fig. 5 for Zn_{1-x}Mn_xTe this results in a disagreement with the high-field data of about 9 meV. This large energy dependence of the transition energies on the Q_c

value is a result of the type-II band alignment and provides a very sensitive determination of the band offset with a resolution of 0.6 meV for every 1% change in Q_c . Since the Zn_{1-x}Mn_xTe layers are wide, the measurement is also relatively insensitive at high fields to the hole mass fitting parameters, due to the small confinement energy. The calculated transition energies for all the samples using $Q_c=0.72$ agree with the experimental data to within 2.5 meV above 15 T. We, therefore, conclude that the conduction band offset ratio is 0.72 ± 0.04 .

V. CONCLUSIONS

In conclusion, we have used magnetorefectivity measurements to probe the Zeeman splitting of the DMS superlattice combination of ZnTe/Zn_{1-x}Mn_xTe. The clear observation of a crossing of the $1s$ exciton from the ZnTe buffer and the lower component of the HH, gives unequivocal evidence of a band alignment change from type I to type II. By extending the measurements to high magnetic field, this allows us to demonstrate the behavior of a type-II exciton, which is in good agreement with the theoretical model presented. From the fitting of the Zeeman splitting, the conduction band offset ratio is found to be 0.72 ± 0.04 .

ACKNOWLEDGMENTS

One of us (H.H.C) wishes to thank Dr. S. L. Wong for helpful discussions. We acknowledge support of this work by EPSRC (U.K.).

¹A. Twardowski, P. Swiderski, M. von Ortenberg, and R. Pauthenet, *Solid State Commun.* **50**, 509 (1984).

²G. Barilero, C. Rigaux, M. Menant, Nguyen Hy Hau, and W. Giriat, *Phys. Rev. B* **32**, 5144 (1985).

³E. Delporte, J. M. Berroir, G. Bastard, C. Delalande, J. M. Hong, and L. L. Chang, *Phys. Rev. B* **42**, 5891 (1990).

⁴E. L. Ivchenko, A. V. Kavokin, V. P. Kochereshko, G. R. Posina, I. N. Uraltsev, D. R. Yakovlev, R. N. Bicknell-Tassius, A. Waag, and G. Landwehr, *Phys. Rev. B* **46**, 7713 (1992).

⁵W. C. Chou, A. Petrou, J. Warnock, and B. T. Jonker, *Phys. Rev. Lett.* **67**, 3820 (1991).

⁶J. Warnock, B. T. Jonker, A. Petrou, W. C. Chou, and X. Liu, *Phys. Rev. B* **48**, 17321 (1993).

⁷J. A. Gaj, R. Planel, and G. Fishman, *Solid State Commun.* **29**, 435 (1979).

⁸E. D. Isaacs, D. Heiman, X. Wang, P. Becla, K. Nakao, S. Takeyama, and N. Miura, *Phys. Rev. B* **43**, 3351 (1991).

⁹R. J. Nicholas, M. J. Lawless, H. H. Cheng, D. E. Ashen-

ford, and B. Lunn, *Semicond. Sci. Technol.* **10**, 791 (1995).

¹⁰H. H. Cheng, R. J. Nicholas, M. J. Lawless, D. E. Ashenford, and B. Lunn (unpublished).

¹¹R. L. Greene and K. K. Bajaj, *Phys. Rev. B* **31**, 6498 (1985).

¹²M. Bugajski, W. Kuszko, and K. Rogiowski, *Solid State Commun.* **60**, 669 (1986).

¹³Chris G. Van de Walle, *Phys. Rev. B* **39**, 1871 (1989).

¹⁴M. Lawless, Ph.D. thesis, Oxford University, 1993.

¹⁵H. Q. Hou, W. Staguhn, S. Takeyama, N. Miura, Y. Segawa, Y. Aoyagi, and S. Namba, *Phys. Rev. B* **43**, 4152 (1991).

¹⁶S. Said and M. A. Kanehisa, *Phys. Status Solidi B* **157**, 311 (1990).

¹⁷N. J. Pulsford, R. J. Nicholas, P. Dawson, K. J. Moore, G. Duggan, and C. T. Foxon, *Phys. Rev. Lett.* **63**, 2284 (1989).

¹⁸B. Kuhn-Heinrich, W. Ossau, T. Litz, A. Waag, and G. Landwehr, *J. Appl. Phys.* **75**, 8046 (1994).

¹⁹S. K. Chang, A. V. Nurmikko, J. W. Wu, L. A. Kolodziejski, and R. L. Gunshor, *Phys. Rev. B* **37**, 1191 (1988).